Real-Time Oil Spill Detection for UAV Images in Varied Terrains in Iraq Based on Deep Learning

Othman Saad Abdulateef and Zaidoon Tareq Abdulwahhab
Department of Computer Science, Computer Science, and Mathematics College, Tikrit University, 34001 Tikrit, Salah Al Deen, Iraq
othmansaad981@gmail.com, ziadoontareq@tu.edu.iq

Keywords: Oil Spill Detection, Deep Learning, Environmental Monitoring, Drone Imagery, YOLOv10.

Abstract: Oil spills pose serious threats to both the environment and public health, demanding fast and accurate detection in all settings. Traditional detection methods are often slow, expensive, and ineffective across diverse terrains. This highlights the urgent need for an efficient, automated solution capable of reliably identifying oil contamination in real time. In this paper, we developed an aerial system using YOLOv10 detector to locate oil contamination on and off the Tigris River banks near Tikrit, Iraq, in real-time. We collected and annotated a custom dataset comprising 700 UAV images, consisting of 470 water-based oil spill images and 230 land-based oil spill images. The images underwent square cropping and normalization, followed by a comprehensive augmentation pipeline that included mosaic mixing and class-aware sample selection. Fine-tuning COCO-pre-trained YOLOv10 weights using freeze-then-unfreeze strategies yielded water-only mAP_{50} results of 69.1 % and land-only 63.1 %. For the combined test set, the detector achieved mAP_{50} 79.7 %. These findings confirm the lightweight UAV platform and the single-stage detector are suitable for extensive real-time environmental monitoring in deprived regions with limited resources.

1 INTRODUCTION

The use of oil and petroleum products greatly increases the possibility of oil and petroleum spilling into water bodies or land, which may adversely affect the environment, natural resources, and public health. It is crucial to detect oil infusion at an early stage in order to prevent damage to sensitive watersheds and industrial water bodies. Oil-centric monitoring methods like satellite imagery, manual inspections greatly lack in area coverage, time efficiency, and safety during ground evaluations [1]. Unmanned aerial vehicles (UAVs) or drones have garnered attention for policy surveillance activities owing to their altitude photography paired with autonomous flight options [2]. Domestic drones, for instance the DJI Mini 2, can achieve altitudes of 5 to 50 meters and provide an incredible precision of less than one meter ground sampling distances, which is ideal for oil spill inspections. Oil-spill UAV- selfies taken under diverse weather, light, and backdrop settings can now be analyzed in real-time using deep-learning object detection frameworks, ensuring timely identification and evaluation of oil-contaminated regions.

The development of Artificial Intelligence (AI) technology and its implementation in a variety of domains has sparked innovation well past the scope of environmental tracking. The use of machine learning (ML) and deep learning (DL) technologies oil spill detection processes has changed remarkably due to the combination of various types of data and improvements in the algorithms used. Some of the initial efforts relied on traditional ML techniques like Support Vector Machines (SVM) and Random Forests (RF). Chen and Lu (2017) [3] incorporated SVM with feature selection that was aware of the subcategory in aerial image oil spill detection and Tong and Chen (2019) [4] used RF on polarimetric Synthetic aperture radar (SAR) data to strengthen detection against noise. Ozigis et al. (2020) [5] also evaluated RF versus Fuzzy Forest (FF) for mapping oil-impacted vegetation and RF's versatility with multispectral and SAR data was emphasized. Feature extraction was done with a machine learning approach using biologically inspired methods of processing with Artificial Neural Networks (ANNs). Park et al. (2020) [6] proved the ability of ANNs in improving the reduction of sun glare in optical sea images. Convolutional Neural Networks (CNNs),

became specialists later as they were better at recognizing spatial patterns. The use of CNNs for characterizing oil slicks in SAR images was pioneered by Guo et al. (2017) [7] while Nieto-Hidalgo et al. (2018) [8] implemented multi-stage CNNs to classify oil spills, ships, and coastlines in radar images. The use of CNNs to large scale oil spill datasets has been reported by Das et al. (2023) [9] which highlights the effectiveness of feature propagation.

Recent advancements in CNN architectures have significantly improved oil spill detection performance in remote sensing applications. Yaohua and Xudong (2019) [10] introduced a DenseNet-based model for SAR image feature extraction and classification using a Softmax layer, tested on ERS-2 SAR data. Wang and Coulson (2023) [11] leveraged a pre-trained MobileNet model, demonstrating the value of transfer learning for custom oil spill detection, particularly on computationally constrained platforms. Zeng and Wang [12] utilized a VGG-16-based DCNN to classify SAR dark spots, with data augmentation enhancing the model's ability to learn features over handcrafted methods. Ronci et al. (2020) [13] extended the U-Net++ architecture by adding a final convolutional layer and training on 839 SAR images from RADARSAT-2 and Sentinel-1. Similarly, Chen et al. (2024) [14] implemented a U-Net model with a lightweight MobileNetv3 backbone, incorporating multi-scale feature fusion to improve class-level feature learning. Krestenitis et al. (2019) [15] explored various DCNNs for semantic segmentation, identifying DeepLabv3+ as the top performer in accuracy and inference speed on oil spill datasets.

Few works combine high-speed detection with UAV mobility in resource-constrained regions. These gaps motivated our use of YOLOv10 with drone imagery to achieve fast, accurate detection across diverse environments, which are listed in Table 1. In this paper, we design and assess an oil spill detection framework based on UAV imagery that processes the YOLOv10 detector for real-time operation on desktop GPUs as well as edge devices. We examine a case study focused on the Tigris River region near Tikrit, Iraq, where recent leaks from pipelines have resulted into observable oil spills on the surface of water as well as stained soil on the adjacent land. Our contributions are:

- A custom dataset of 700 UAV images containing water-only and land-only oil spills with varying backgrounds, including complex environmental conditions.
- A comprehensive preparatory pipeline that includes normalization, augmentation using mosaic mixing, photometric and geometric transforms, as well as class-aware sampling aimed at increasing model robustness.
- Oil spill detection-specific fine-tuning strategies for YOLOv10 including freeze-then-unfreeze and custom anchor estimation.
- Comprehensive analysis measuring mean Average Precision reported mAP@50 with water-only, land-only, and combined test sets.

Table 1: Related work with different remote sensing images.

Ref.	Data	Method	Remarks
[3]	Sea water images	SVM	Data reliability is low
[4]	SAR (Radarsat-2, UAVSAR)	RF	Accuracy up to 92.99%
[5]	Multifrequency SAR	FF, RF	Accuracy 75%
[6]	Optical satellite (KOMPSAT-2)	ANN	Reliability is limited
[7]	Polarimetric SAR	CNNs	Sea state variation affects accuracy
[8]	Side-looking airborne radar images	CNNs	No major improvement in spill detection
[9]	SAR images	CNNs	Depends on image quality
[10]	SAR (ERS-2)	DenseNet	Oil-like films not considered
[11]	Remote sensing images	MobileNet	Dataset lacks full spill variation
[12]	SAR (dark patches)	VGG16	Workload is heavy
[13]	SAR (Radarsat-2, Sentinel-1)	UNet	Need better post-processing
[14]	SAR (MKLab)	U-Net + MobileNetv3	mIoU >80%
[15]	SAR images	DeepLabv3+	mIoU 65.06%
[16]	SAR (Sentinel-1)	YOLOv4	AP 68.69% but weak performance in new area
[17]	SAR (DM4D dataset)	YOLOv8	mIoU 69.52%
[18]	UAV imagery	RF	Accuracy 77%
[19]	UAV imagery	CNN	Accuracy 83.3%

2 MATERIALS AND METHODS

The methodology involves collecting drone images of oil-contaminated land and water, then performing image enhancements and robust training of the YOLOv10 model. Its accuracy will be evaluated and validated in a variety of environmental conditions.

2.1 Dataset Collection and Curation

The dataset was obtained while performing field activities on two adjacent sections of Tigris River near Tikrit Iraq. The first zone included riverine segments with documented leaks from pipelines affected by intermittent oil sheen and patchy slicks on the water surface as shown in Figure 1. The second zone included industrial lands located on the eastern side of the river with contaminated soils near the storage tanks and pipeline corridors as shown in Figure 2.

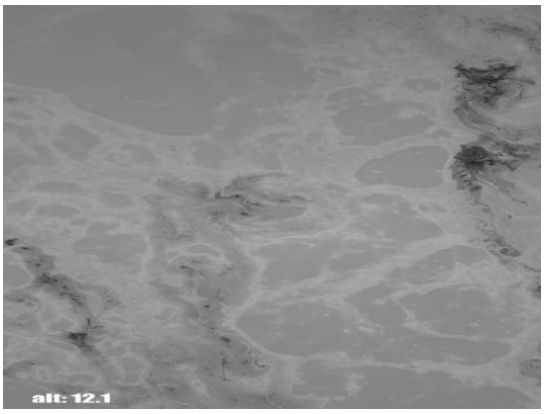

Figure 1: Aerial drone imagery contrasting oil-polluted and contaminated water zones.

Figure 2: Drone-acquired aerial views of terrestrial landscapes.

A DJI Mini 2 quad-rotor outfitted with 12.0 MP RGB camera captured images while hovering between 5 meters and 50 meters AGL. Flights were done under varying weather conditions such as:

- Shadow illumination: full sun, partially cloudy, over cast.
- Water conditions: still, wind ripples, constant changes in water clarity.
- Background terrains: sandy loam, clay, mixed aggregates, shadowed, and non-shadowed from adjacent structures.

The cameras were preset to 4K (3840×2160 pixels) and 24 fps which guarantee the absence of noise at ISO 100. A total of 700 images were taken, 470 of which were oil contamination on the water surface only, while the rest 230 were from the oil-stained soil and debris on land. The dataset's geographic focus was necessary for controlled data collection under known spill conditions, ensuring annotation accuracy. While this limits diversity, the model was trained with strong augmentations and mixed scenarios to encourage broader generalization.

2.2 Ground Truth Annotation

Annotation of images took place on the RoboFlow platform. Annotations were done in the YOLO format, with water oil as (class 0) and land oil (class 1) as the two classes. Additionally, normalized center coordinates along with the dimensions of the bounding boxes were created for every image. Expert annotators tightly defined the bounding boxes of the following features:

- Water-based oil. continuous sheens, discrete patches, and emulsified areas as shown in Figure 3.
- Land-based oil. stained soil, runoff streaks, and oil-soaked debris as shown in Figures 3 and 4.

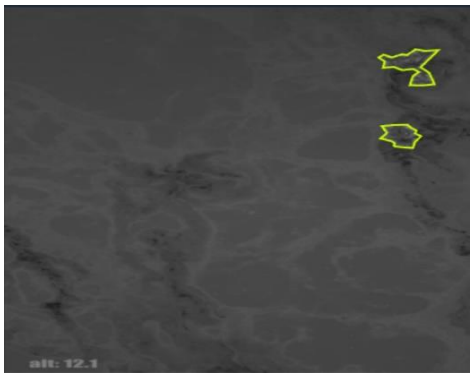

Figure 3: Example of annotating a water-based oil image using the platform.

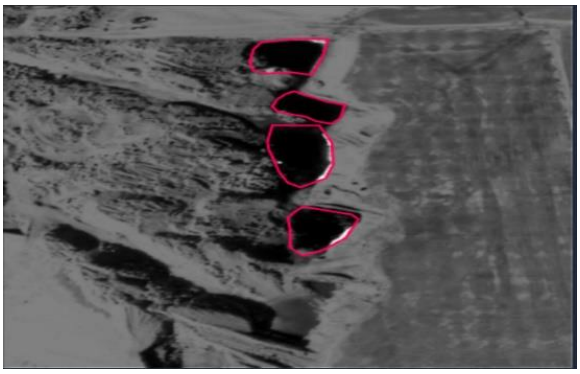

Figure 4: Example of annotating a land-based oil image using the platform.

2.3 Data Splitting Strategy

Multiple data splitting scenarios were tested across water, land, and combined (water-land) datasets to identify optimal performance. After evaluating 66 parameter configurations, the best results were achieved with the following splits:

- Water Data. 75% training, 23% validation, and 2% testing.
- Land Data. 76% training, 22% validation, and 2% testing.
- Water-Land Data. 84% training, 15% validation, and 1% testing.

The testing sets were intentionally kept small to maximize training data availability, which is crucial for learning in data-limited scenarios like environmental monitoring. Our primary aim was to improve model generalization through diverse training and validation exposure while using held-out test samples only for final benchmarking. The data partitioning strategy was tailored to the unique characteristics and sample sizes of each subset to ensure sufficient representation of critical features during training. For the combined water-land dataset, a larger training proportion (84%) was necessary to capture the increased complexity and variability across domains. Although the splits differ slightly, each configuration was optimized through empirical testing to balance learning capacity and validation reliability within the constraints of limited data.

2.4 Preprocessing and Augmentation

The following steps were taken for all images prior to training:

- Quality filtering. Exclude images with drastic motion blur, over-exposure, under-exposure, or lens artifacts (<2% of data).
- Uniform square cropping. Center-crop to maintain a square aspect ratio.
- Resizing. Resizing to 640×640 was chosen to ensure compatibility with YOLOv10 while maintaining processing efficiency and consistent input dimensions across batches. Although domain-specific augmentations could further improve generalization, the current pipeline prioritizes general-purpose enhancements to retain dataset balance and model scalability.
- Normalization. Adjust pixel values to [0,1] range. Perform mean subtraction and standard deviation normalization per channel using ImageNet parameters.

An augmentation pipeline executed as follow:

- Geometric transforms. Horizontal and vertical flips, rotation of ±15°, scale from 0.8 to 1.2.
- Photometric jitter. Change brightness and contrast ± 20, change saturation ± 15, Gaussian blur with $\sigma \leq 1.0$.
- Mosaic mixing. Four images per sample are combined using box clipping and area-based filtering.
- Class-aware sampling. Guarantee every minibatch (size 16) has a minimum of >3 water_oil images.

To address class imbalance, class-aware sampling was implemented to ensure each training mini-batch included at least three water-based samples. Additionally, balanced data splits and augmentation were applied to prevent model bias toward the dominant aquatic class. This dataset along with the described preprocessing steps provides a solid basis for training and testing the YOLOv10 detector in aquatic and terrestrial spill scenarios.

2.5 Model Development

YOLOv10 is a state-of-the-art, real-time object detection algorithm designed for fast and accurate detection. It builds on previous YOLO versions by improving backbone efficiency, multi-scale feature fusion, and detection heads, enabling better performance in detecting small and complex objects in diverse environments. We adopted the YOLOv10 variant optimized for fast inference and balanced detection accuracy, making it suitable for UAV-based oil spill monitoring:

- The architecture begins with a CSP-Darknet backbone, which extracts hierarchical features while reducing computational burden.

- This is followed by a Spatial Pyramid Pooling (SPP) module that captures multi-scale spatial context, critical for identifying variable oil spill patterns.
- A PANet neck is then employed to enhance feature fusion across scales, improving the model's ability to localize spills in both water and land environments.
- Detection is performed using three output heads operating at strides of 8, 16, and 32, enabling accurate recognition of small to large spill regions.
- The model is initialized with COCO-pretrained weights, which help bootstrap training by providing rich low-level features, thus accelerating convergence and improving early-stage performance on oil-specific imagery.

The training process was conducted on an NVIDIA RTX 3090 GPU using the Adam optimizer. The most important hyperparameters are:

- Learning rate: Initial 0.001, decayed to 0.00001 using cosine annealing.
- Weight decay: 0.0005.
- Batch size: 16 images per iteration.
- Precision: In an effort to accelerate computation and reduce memory usage, mixed-precision training (fp16) was used.

A freeze-then-unfreeze strategy was employed, where the first two backbone CSP stages were frozen for the first 10 epochs to retain pre-trained features, then all layers were unfrozen for the remaining 90 epochs. The strategy was adopted based on established practices in transfer learning to retain low-level features from COCO pretraining. It aimed to stabilize early training and accelerate convergence given limited domain-specific data. The composite loss function consists of:

- Bounding box regression loss (CIoU): accuracy in localization is reasoned spatially.
- Classification loss (CE): cross entropy loss for two classes.
- DFL: Distribution Focal Loss – improves bounding box estimates.

The combined use of CIoU, CE, and DFL losses was adopted based on established best practices to improve localization and classification accuracy.

The development process includes evaluation of training and validation losses (box, classification, DFL) as well as mean Average Precision (mAP@50 and mAP@[.5:.95]) with the validation set. The best model checkpoint was selected based on the highest mAP@[.5:.95].Also, class-aware sampling was implemented in such a way that at least three water oilers were present in each mini-batch to reduce class imbalance. The final assessment was performed on three held-out test sets: Water-only set, Land-only set and combined set.

The metrics reported include mAP@50, mAP@[.5:.95] and average IoU for true positives. Parameters such as learning rate schedules, weight decay, and batch size were optimized via grid search on validation set aimed to maximize mAP@ [.5:.95]. This training regimen was aimed for the YOLOv10 model to achieve high-speed and high-accuracy oil spill detection across varying conditions.

3 RESULTS AND EVALUATION

The experimental evaluation of YOLOv10 across three test scenarios—Land-only, Water-only, and Combined (Water + Land)—reveals distinct performance trends, as summarized in Table 2. The model achieved its highest mean Average Precision (mAP@50) of 79.7% in the combined scenario, demonstrating the advantages of training on diverse datasets that incorporate both aquatic and terrestrial environments. This suggests that exposure to varied textures, such as oil sheens on water and irregular patches on land, enhances the model's ability to generalize and reduces overfitting to domain-specific noise. In contrast, the Water-only scenario yielded a moderate mAP@50 of 69.1%, reflecting challenges posed by dynamic water conditions like sun glint, wave interference, and algae blooms, which often mimic oil sheens and lead to false positives. The Land-only scenario performed weakest at 63.1%, underscoring the complexities of terrestrial environments, where shadows, industrial debris, and overlapping textures (e.g., wet soil or rust) complicate spill detection, particularly for smaller spills (<1m²) due to limited spatial resolution.

Table 2: Comparing the performance for the three scenarios.

Scenario	mAP@50 (%)
Land-only	63.1
Water-only	69.1
Combined (Water + Land)	79.7

3.1 Training Curve Analysis

We tracked key training and validation metrics over 100 epochs for each scenario:

- Land-only curves: The model exhibited rapid convergence, with train/cls_loss falling from

~25 to below 3 by epoch 10, and val/mAP@50 surpassing 0.85 around epoch 60. Training precision approached 0.85 and recall neared 0.9, reflecting high detection consistency on high-contrast land spills.

- Water-only curves: Training and validation box, classification, and DFL losses showed an overall decrease, with the most cls_loss reduction occurring in the first ten epochs. Precision improved from ~0.4 to over 0.8, and recall improved from ~0.3 to ~0.7, suggesting some useful feature learning was taking place despite water reflection interference.
- Combined curves: Loss curves decreased more gradually and had occasional oscillations in precision because of the heterogeneity in the object appearance. By epoch 80, Val/mAP@50 reached ~0.7 and mAP@50-95 stabilized around 0.28, demonstrating learning adaptability across both domains.

Across the board, the attention and tracking disciplines mastered in synched training have cross-domain applicability, as demonstrated by the close spacing between the training and validation curves across all scenarios. These patterns support the effectiveness of the implemented freeze-unfreeze method and augmentation pipeline. In summary, the model performs well in the Water-Land scenario but shows slightly reduced accuracy and more variability in precision compared to the Water-only scenario. These differences are expected due to the increased complexity and diversity of the mixed environment, which introduces additional challenges in object detection.

3.2 Qualitative Analysis

By virtue of visually inspecting the document, two overriding error modes can be noted as follows:

- Low water sheen contrast: Oil films on rippled or turbid water sometimes resulted in missed detections or low-confidence outputs using thin water sheens.
- Background confusion: Some shadows dark on soil or wet asphalt occasionally resulted in false positives.

Due to logistical and environmental constraints, external datasets were not available; thus, diverse real-world conditions were simulated within the existing dataset to encourage generalizability. The split strategy ensured varied representation across training and validation sets to approximate unseen scenarios. Figure 5 show casing oil spill detection using yolo10 on land data. Figure 6 showcasing oil spill detection using Yolo10 on water data.

Figure 5: Oil spill detection using yolo10 on land data.

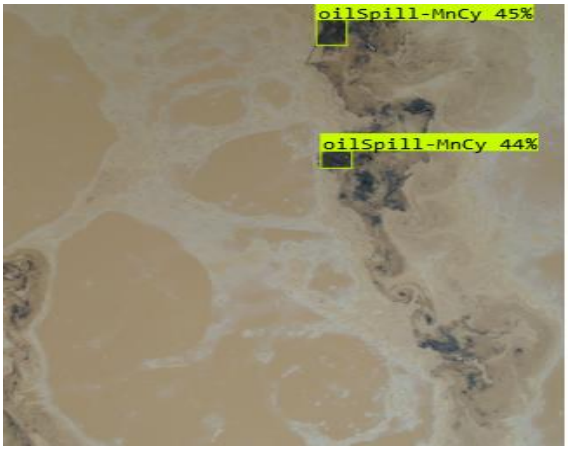

Figure 6: Oil spill detection using yolo10 on water data.

Our study is closely related to SAM-OIL in [17], which uses semantic segmentation based on SAR images, but it surpasses it in several key areas. Unlike SAM-OIL, which requires extensive pixel-level annotations and a multi-stage process involving YOLOv8, SAM, and OMF, our method uses YOLOv10 with simple bounding box annotations, reducing annotation complexity and computational overhead. Our model is optimized for real-time deployment on UAVs using RGB imagery, making it more practical and scalable. While SAM-OIL focuses on fine-grained segmentation, our approach achieves competitive detection accuracy with a streamlined architecture. Moreover, by addressing diverse terrain types and ensuring domain adaptability, our model offers broader generalization and deployment readiness.

4 CONCLUSIONS

In this paper, we showed that real-time detection of oil spills on water and land surfaces is possible using a lightweight YOLOv10 model deployed on UAV captured images. Our framework reached mAP@50 of 69.1% (water only), 63.1% (land only), and 79.7% (combined) while achieving over 65 FPS on desktop GPUs and 25 FPS on edge devices. These findings support the notion that resource-limited detectors are capable of providing usable accuracy value for real-time environmental monitoring under in situ conditions.

While our approach achieved strong results, a number of challenges remain. First, detection accuracy diminishes with thinner, low-contrast oil sheen layers on highly reflective turbid water due to missed detections. Dark shadows and visually indistinguishable backgrounds on land can also create false positives. Moreover, the focus of our study is RGB data, which limits performance in more sophisticated situations where other spectral data would improve separation. To overcome these limitations, further research should investigate:

- The addition of near infrared, thermal or SAR data to increase the discrimination value of oil against the background and reduce misses and false alarms.
- Using video clips together with spatial and temporal smoothing to stabilize detections and reduce flicker during the subsequent processing of videos captured by UAVs.
- Semi-supervised and active learning: Enhancing dataset creation by using strategies such as pseudo-labeling, domain adaptation, or human-in-the-loop, which help to improve consistency across different scenarios, requiring only minimal annotation effort.
- Instance segmentation extension: I ntegrating segmentation models such as YOLO with SAM to capture and define the exact spill boundaries to achieve more precise area quantification.

As we made clear above, the UAV based YOLOv10 pipeline we developed enables oil spill monitoring in low resources setting with unprecedented speed and at a fraction of the cost, demonstrating remarkable flexibility and scalability. Focusing on model efficiency and real-time execution allows the framework to assist environmental agencies and first responders with early detection and mitigation strategies. Dedicated work in the directions outlined above is expected to further increase the confidence and widen the use of detection across diverse ecological and industrial environments.

REFERENCES

[1] U. Singh, D. Acharya, and S. Mishra, “Oil spill detection and monitoring with artificial intelligence: A futuristic approach,” in Proc. World Conf. Eng. Sci. (WCES), Apr. 2022, pp. 12–22.

[2] Z. Jiao, G. Jia, and Y. Cai, “A new approach to oil spill detection that combines deep learning with unmanned aerial vehicles,” Comput. Ind. Eng., vol. 135, pp. 1300–1311, 2019.

[3] T. Chen and S. Lu, “Subcategory-aware feature selection and SVM optimization for automatic aerial image-based oil spill inspection,” IEEE Trans. Geosci. Remote Sens., vol. 55, no. 9, pp. 5264–5273, Sep. 2017.

[4] S. Tong, X. Liu, Q. Chen, Z. Zhang, and G. Xie, “Multi-feature based ocean oil spill detection for polarimetric SAR data using random forest and the self-similarity parameter,” Remote Sens., vol. 11, no. 4, p. 451, Feb. 2019.

[5] M. S. Ozigis, J. D. Kaduk, C. H. Jarvis, P. da Conceição Bispo, and H. Balzter, “Detection of oil pollution impacts on vegetation using multifrequency SAR, multispectral images with fuzzy forest and random forest methods,” Environ. Pollut., vol. 256, p. 113360, Mar. 2020.

[6] S. H. Park, H. S. Jung, and M. J. Lee, “Oil spill mapping from Kompsat-2 high-resolution image using directional median filtering and artificial neural network,” Remote Sens., vol. 12, no. 2, p. 253, Jan. 2020.

[7] H. Guo, D. Wu, and J. An, “Discrimination of oil slicks and lookalikes in polarimetric SAR images using CNN,” Sensors, vol. 17, no. 8, p. 1837, Aug. 2017.

[8] M. Nieto-Hidalgo, A. J. Gallego, P. Gil, and A. Pertusa, “Two-stage convolutional neural network for ship and spill detection using SLAR images,” IEEE Trans. Geosci. Remote Sens., vol. 56, no. 9, pp. 5217–5230, Sep. 2018.

[9] K. Das, P. Janardhan, and H. Narayana, “Application of CNN based image classification technique for oil spill detection,” Indian J. Geo-Mar. Sci., vol. 52, no. 1, pp. 5–14, Jan. 2023.

[10] X. Yaohua and M. Xudong, “A SAR oil spill image recognition method based on densenet convolutional neural network,” in Proc. Int. Conf. Robots Intell. Syst. (ICRIS), Jun. 2019, pp. 78–81.

[11] C. Wang and A. Coulson, “Fine tuning MobileNet neural networks for oil spill detection,” unpublished, 2023.

[12] K. Zeng and Y. Wang, “A deep convolutional neural network for oil spill detection from spaceborne SAR images,” Remote Sens., vol. 12, no. 6, p. 1015, Mar. 2020.

[13] F. Ronci, C. Avolio, M. Di Donna, M. Zavagli, V. Piccialli, and M. Costantini, “Oil spill detection from SAR images by deep learning,” in Proc. IEEE Int. Geosci. Remote Sens. Symp. (IGARSS), Sep. 2020, pp. 2225–2228.

[14] Y. T. Chen, L. Chang, and J. H. Wang, "Full-scale aggregated MobileUNet: An improved U-Net architecture for SAR oil spill detection," Sensors, vol. 24, no. 12, p. 3724, Jun. 2024.

[15] M. Krestenitis, G. Orfanidis, K. Ioannidis, K. Avgerinakis, S. Vrochidis, and I. Kompatsiaris, "Oil spill identification from satellite images using deep neural networks," Remote Sens., vol. 11, no. 15, p. 1762, Aug. 2019.

[16] Y. J. Yang, S. Singha, and R. Mayerle, "A deep learning based oil spill detector using Sentinel-1 SAR imagery," Int. J. Remote Sens., vol. 43, no. 11, pp. 4287–4314, Jun. 2022.

[17] W. Wu, M. S. Wong, X. Yu, G. Shi, C. Y. T. Kwok, and K. Zou, "Compositional oil spill detection based on object detector and adapted Segment Anything model from SAR images," IEEE Geosci. Remote Sens. Lett., in press, 2024.

[18] M. Mahdianpari, B. Salehi, F. Mohammadimanesh, G. Larsen, and D. R. Peddle, "Mapping land-based oil spills using high spatial resolution unmanned aerial vehicle imagery and electromagnetic induction survey data," J. Appl. Remote Sens., vol. 12, no. 3, Art. no. 036015, Jul. 2018.

[19] U. F. Ukaegbu, L. K. Tartibu, M. O. Okwu, and I. O. Olayode, "Integrating unmanned aerial vehicle and deep learning algorithm for pipeline monitoring and inspection in the oil and gas sector," in Proc. Int. Conf. Artif. Intell. Appl., Dec. 2021, pp. 1–6.